ISSN 1674-1056
http://cpb.iphy.ac.cn
http://iopscience.iop.org/cpb
中国物理 B
Chinese Physics
中国物理 Chinese Physics B

# First-principles investigations on structural stability, mechanical, and thermodynamic properties of La$T_2$Al$_{20}$ ($T$=Ti, V, Cr, Nb, and Ta) intermetallic cage compounds

Shanyu Quan(权善玉), Xudong Zhang(张旭东), Cong Liu(刘聪), Wei Jiang(姜伟)

**Citation:**Chin. Phys. B . 2018, 27(12): 126201. **doi:** 10.1088/1674-1056/27/12/126201
Journal homepage: http://cpb.iphy.ac.cn; http://iopscience.iop.org/cpb

**What follows is a list of articles you may be interested in**

---

## Effects of alloying element on stabilities, electronic structures, and mechanical properties of Pd-based superalloys

Pei Yan(闫佩), Xiao-Yu Chong(种晓宇), Ye-Hua Jiang(蒋业华), Jing Feng(冯晶)

Chin. Phys. B . 2017, 26(12): 126202. **doi:** 10.1088/1674-1056/26/12/126202

## Investigation of mechanical properties of twin gold crystal nanowires under uniaxial load by molecular dynamics method

Guo-Wei Zhang(张国伟), Zai-Lin Yang(杨在林), Gang Luo(罗刚)

Chin. Phys. B . 2016, 25(8): 086203. **doi:** 10.1088/1674-1056/25/8/086203

## First-principles calculation of the structural, electronic, elastic, and optical properties of sulfur-doping $\varepsilon$-GaSe crystal

Chang-Bao Huang(黄昌保), Hai-Xin Wu(吴海信), You-Bao Ni(倪友保), Zhen-You Wang(王振友), Ming Qi(戚鸣), Chun-Li Zhang(张春丽)

Chin. Phys. B . 2016, 25(8): 086201. **doi:** 10.1088/1674-1056/25/8/086201

## Mechanical and thermodynamic properties of cubic $YH_2$ under high pressure：Prediction from first-principles study

Li Zhen-Li, Cheng Xin-Lu

Chin. Phys. B . 2014, 23(4): 046201. **doi:** 10.1088/1674-1056/23/4/046201

## Pressure dependences of elastic and lattice dynamic properties of AlAs from *ab initio* calculations

Li Xing-Xiu, Tao Xiao-Ma, Chen Hong-Mei, Ouyang Yi-Fang, Du Yong

Chin. Phys. B . 2013, 22(2): 026201. **doi:** 10.1088/1674-1056/22/2/026201

---

# First-principles investigations on structural stability, mechanical, and thermodynamic properties of $LaT_2Al_{20}$ ($T$ = Ti, V, Cr, Nb, and Ta) intermetallic cage compounds*

Shanyu Quan(权善玉)[1], Xudong Zhang(张旭东)[1,†], Cong Liu(刘聪)[1], and Wei Jiang(姜伟)[1,2]

[1] School of Science, Shenyang University of Technology, Shenyang 110870, China
[2] School of Materials Science and Engineering, Shenyang University of Technology, Shenyang 110870, China

(Received 15 August 2018; revised manuscript received 9 October 2018; published online 25 November 2018)

First principles calculations were used to explore the structural stability, mechanical properties, and thermodynamic properties of $LaT_2Al_{20}$ ($T$ = Ti, V, Cr, Nb, and Ta) intermetallics. The calculated formation enthalpy and phonon frequencies indicate that $LaT_2Al_{20}$ intermetallics exhibit the structural stability. The elastic moduli ($B$, $G$, $E$, and $H_v$) indicate that these intermetallics possess the better elastic properties than pure Al. The values of Poisson's ratio $v$ and $B/G$ demonstrate that $LaT_2Al_{20}$ intermetallics are all brittle materials. The anisotropy of elasticity and Young's modulus (three- and two-dimensional figures) indicate that $LaT_2Al_{20}$ compounds are anisotropic. Importantly, the calculated thermal quantities demonstrate that $LaT_2Al_{20}$ intermetallics possess the better thermal physical properties than pure Al at high temperatures.

**Keywords:** $LaT_2Al_{20}$ intermetallics, mechanical properties, anisotropic properties, dynamical and thermodynamic properties, first-principles calculations

**PACS:** 62.20.–x, 61.90.+d, 62.20.D– **DOI:** 10.1088/1674-1056/27/12/126201

## 1. Introduction

Aluminum alloys have been playing an important role in many industrial fields due to their outstanding physical properties.[1] But the poor creep-resistance properties of aluminum alloys have hindered their wide applications at high temperatures. In the past few decades, many researchers found that the addition of appropriate transition metal elements (TM) and rare earth elements (RE) to aluminum alloys can form $L1_2$, $D0_{22}$, $D0_{23}$ or $D0_{19}$-ordered binary $Al_3TM$ and $Al_3RE$ intermetallics. These binary intermetallics exhibit some outstanding physical properties, including low mass densities, high melting points, and good oxidation resistances, and so on, which can effectively improve the poor creep-resistance of aluminum alloys.[2–15] In the meantime, some ternary $AT_2Al_{20}$ intermetallics systems (where $A$ = actinide/lanthanide/calcium and $T$ = transition metal) were synthesized with $CeCr_2Al_{20}$-type structure.[16–32] Kangas and Thiede synthesized the new $LaT_2Al_{20}$ ($T$ = Ti, V, Cr, Nb, and Ta) intermetallics by using a step-wise arc melting technique and by self-flux method.[31,32] For these new $LaT_2Al_{20}$ phases, although their intrinsic physical properties have been explored, their mechanical properties and thermodynamics properties are not clarified. It is necessary to investigate the related physical properties for further applications. In the present work, the first-principles calculations were used to comparatively investigate the structural stability, mechanical, and thermodynamics properties for Al and $LaT_2Al_{20}$ intermetallics.

## 2. Computational methods

The first-principles calculations were performed by using the VASP code based on the density functional theory (DFT). The electron–ion interaction and the exchange–correlation energy were described under the projector-augmented wave (PAW) method and the generalized gradient approximation (GGA) of Perdewe–Burkee–Ernzerhof (PBE) scheme, respectively.[33] The f electrons of La atom were frozen into the core states in PAW potentials. The energy cut off for the plane wave basis is 600 eV for all compounds. The $9\times9\times9$ $k$-points for $LaT_2Al_{20}$ unit cell with the Monkhorst–Pack scheme were constructed for the Brillouin zone sampling. Spin polarization was used in the present calculations. The phonon dispersions, density of states, and thermodynamics quantities were calculated by using the supercell method and linear response method with PHONOPY code.[34] The stress–strain method was used to calculate the elastic constants of $LaT_2Al_{20}$ intermetallics.[35]

## 3. Results and discussion

### 3.1. Structural stability

$LaT_2Al_{20}$ intermetallics can crystallize in the face-centered cubic structure with $Fd$-3$m$ space group. In the prototypic $LaT_2Al_{20}$ compounds, La atoms occupy the 8$a$ Wyckoff sites, $T$ atoms occupy the 16$d$ Wyckoff sites, and Al atoms occupy the 16$c$, 48$f$, and 96$g$ Wyckoff sites. The unit cell of

*Project supported by the Program for Ph. D Start-up Fund of Liaoning Province of China (Grant No. 201601161).
†Corresponding author. E-mail: zxdwfc@163.com
© 2018 Chinese Physical Society and IOP Publishing Ltd 

structure is shown in Fig. 1.[25] The optimized atom coordinates are listed in Table 1, together with experimental ones. In the meantime, the ratios of volume change ($V/V_0$) under different pressures were shown in Fig. 2. In Table 1, the calculated data are slightly larger than experimental ones[31,32] and the error is less than 5%, which indicates that the computational method is reliable. $LaNb_2Al_{20}$ has the largest bulk modulus $B_0$ among five intermetallics, which indicates the $LaNb_2Al_{20}$ has the best ability to resist the compression. In Fig. 2, the curves of $V/V_0$ are smooth and have no inflection points until 50 GPa, which indicates that these intermetallics can keep structural stability under high pressures. The curves of $LaNb_2Al_{20}$ and $LaV_2Al_{20}$ locate at upper part and lower part, which indicates that $LaNb_2Al_{20}$ and $LaV_2Al_{20}$ have the best/worst resistance ability to compression among five compounds.

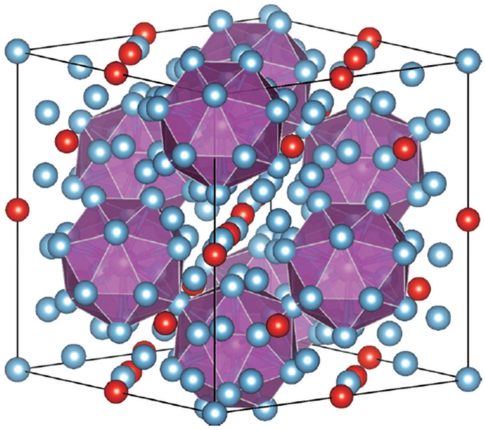


**Fig. 1.** (color online) Crystal structure of $LaTAl_{20}$ intermetallics with $CeCr_2Al_{20}$-type structure. The violet balls are La atoms, the red balls are $T$ atoms, and the blue balls are Al atoms.

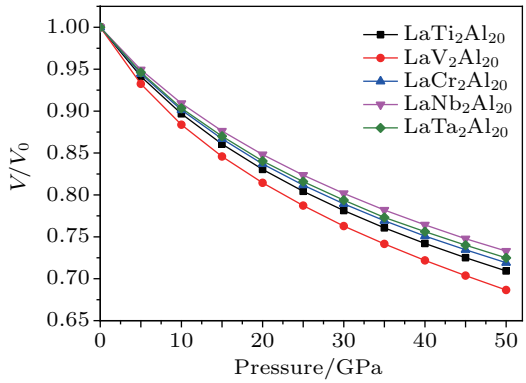



**Fig. 2.** (color online) Equation of state for $LaT_2Al_{20}$ intermetallics.

Generally speaking, the structural stability of the solid materials mainly depends on two conditions: one is thermodynamic condition, which depends on the formation enthalpy; the other is the dynamical condition, which depends on the phonon frequencies.[36,37] The formation enthalpy was calculated using the following expression[38–41]

$$\Delta H = \frac{E_{\text{Total}} - xE_{\text{La}} - yE_{\text{T}} - zE_{\text{Al}}}{x+y+z}, \quad (1)$$

where $E_{\text{Total}}$ represents the total energy of $LaT_2Al_{20}$; $x$, $y$, and $z$ are the numbers of atoms in the unit cell; $E_{\text{La}}$, $E_{\text{T}}$, and $E_{\text{Al}}$ represent the total energy of per atom in solids. The calculated formation enthalpies $\Delta H$ for $LaT_2Al_{20}$ are all negative values in Table 1, indicating that $LaT_2Al_{20}$ compounds have the stronger thermodynamic stability and is more inclined to form $LaTa_2Al_{20}$ due to the lower value of $\Delta H$.

**Table 1.** The lattice constant $a_0$, bulk modulus $B_0$ and formation enthalpy. $\Delta H$ of $LaT_2Al_{20}$ ($T$ = Ti, V, Cr, Nb, and Ta) intermetallics.

| Compounds | $a$/Å | $B_0$/GPa | $\Delta H$/(eV/atom) | |
|---|---|---|---|---|
| $LaTi_2Al_{20}$ | 14.912 | 78.192 | –0.3213 | this work |
| | 14.7713 | | | Exp.[31] |
| $LaV_2Al_{20}$ | 14.788 | 65.665 | –0.3325 | this work |
| | 14.60 | | | Exp.[31] |
| $LaCr_2Al_{20}$ | 14.632 | 87.026 | –0.3334 | this work |
| | 14.45 | | | Exp.[32] |
| $LaNb_2Al_{20}$ | 15.062 | 88.367 | –0.3395 | this work |
| | 14.811 | | | Exp.[32] |
| $LaTa_2Al_{20}$ | 15.081 | 88.012 | –0.3398 | this work |
| | 14.811 | | | Exp.[32] |

In order to explore the dynamical stability, the phonon dispersion and the density of states are calculated in Figs. 3 and 4. The solid lines are calculated values and the scatter points are experimental ones of the inelastic neutron scattering measurement in Fig. 3.[42] The calculated values are close to the experimental ones, which indicate that the calculated results are reasonable. Figure 4 shows the phonon dispersion curves and the density of states for $LaT_2Al_{20}$ intermetallics. For five figures of phonon dispersion curves, the imaginary phonon frequencies are absent along the Brillouin zone path. It indicates that the five compounds possess the dynamical stability. Figure 5 displays the total phonon density of states for $LaT_2Al_{20}$ intermetallics. For the phonon density of states (PHDOS), the imaginary frequencies are also absent. It indicates that the five compounds possess the dynamical stability. In summary, according to the obtained formation enthalpies and phonon frequencies, the five intermetallics exhibit the structural stability.

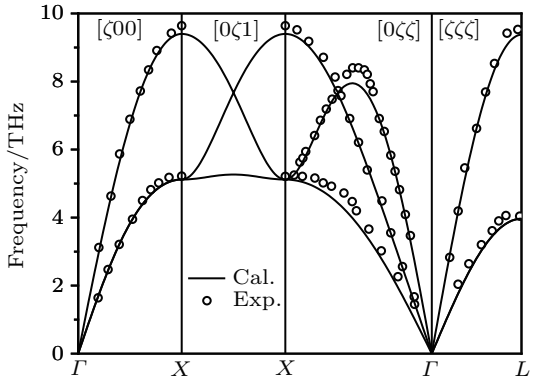



**Fig. 3.** Phonon dispersion curves of Al and the circles correspond to the experimental data.

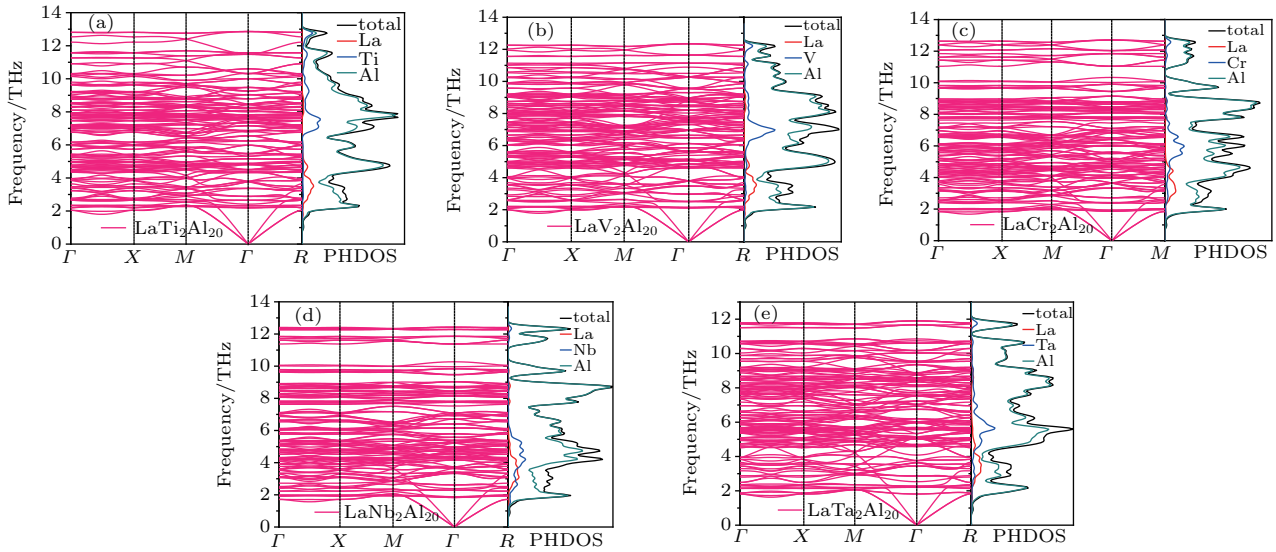



**Fig. 4.** (color online) Phonon dispersion curves and density of states for $LaT_2Al_{20}$ intermetallics.

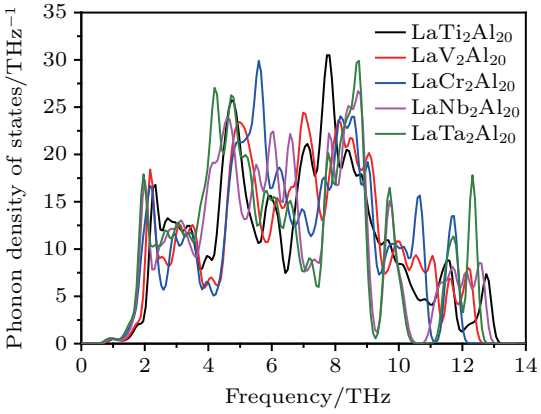



**Fig. 5.** (color online) The total phonon density of states for $LaT_2Al_{20}$ intermetallics.

### 3.2. Elastic properties

The elastic constants and elastic moduli are important parameters for engineering applications. Table 2 listed the calculated elastic constants $C_{ij}$ and compliance matrices $S_{ij}$, together with the experimental values of pure Al for comparison.[43–45] The elastic constants of Al are consistent with experimental ones (as shown in Table 2). The calculated results indicate that our computational method is reliable. For the cubic structure intermetallics, there are three independent constants $C_{11}$, $C_{12}$, and $C_{44}$. The elastic constants are satisfied with the mechanically stable conditions:[46] $C_{11} > 0$, $C_{44} > 0$, $C_{11} > |C_{12}|$, $(C_{11} + 2C_{12}) > 0$. After obtaining the elastic constants $C_{ij}$ and $S_{ij}$, the bulk modulus $B$, shear modulus $G$, Young's modulus $E$, and hardness $H_v$ were calculated by using the VRH method with the following equations[46]

$$B_V = \frac{1}{3}C11 + \frac{2}{3}C_{12}, \quad B_R = \frac{1}{3S_{11} + 6S_{12}},$$
$$B = \frac{1}{2}(B_V + B_R), \tag{2}$$

$$G_V = \frac{1}{5}C11 - \frac{1}{5}C_{12} + \frac{3}{5}C_{44}, \quad \frac{5}{G_R} = \frac{4}{C_{11} - C_{12}} + \frac{3}{C_{44}},$$
$$G = \frac{1}{2}G_V + \frac{1}{2}G_R, \tag{3}$$
$$E = \frac{9BG}{3B + G}, \quad v = \frac{3B - 2G}{2(3B + G)},$$
$$H_V = 0.92G^{0.708}(G/B)^{1.137}. \tag{4}$$

The calculated elastic moduli of $LaT_2Al_{20}$ are listed in Tables 3 and 4, together with the experimental ones of Al.[43,45] The bigger values of bulk modulus $B$ and shear modulus $G$ correspond to the better resistance of solid materials against volume change under hydrostatic pressure and shape deformation by the shearing force. In Table 3, the values of elastic modulus $B$ follow the order: $LaNb_2Al_{20} > LaTa_2Al_{20} > LaCr_2Al_{20} > Al > LaTi_2Al_{20} > LaV_2Al_{20}$, this indicates that $LaNb_2Al_{20}$ has the best ability of resistance to the volume deformation. The values of elastic modulus $G$ follow the order: $LaNb_2Al_{20} > LaTi_2Al_{20} > LaTa_2Al_{20} > LaV_2Al_{20} > LaCr_2Al_{20} > Al$, indicating that $LaNb_2Al_{20}$ has the best ability of resistance to shape change under external conditions. Five $LaT_2Al_{20}$ intermetallics have the stronger shear deformation resistance in comparison with the pure Al. The larger elastic constants $C_{44}$, elastic modulus $G$, and $E$ correspond to the higher hardness of solid materials. The values of $C_{44}$, $G$, and $E$ of five intermetallics are remarkably larger than the ones of pure Al, indicating that these ternary intermetallics possess the higher hardness than the pure Al. In the meantime, for $LaTi_2Al_{20}$, $LaV_2Al_{20}$, $LaCr_2Al_{20}$, $LaNb_2Al_{20}$, $LaTa_2Al_{20}$, and Al, the values of hardness are also calculated by using the semi-empirical equations with Eq. (4): 12.249 GPa, 12.191 GPa, 7.747 GPa, 12.590 GPa, 9.359 GPa, and 2.868 GPa. The calculated results indicate the $LaT_2Al_{20}$ compounds are harder than Al.

**Table 2.** Calculated elastic constants $C_{ij}$ (in unit GPa) and compliance matrices $S_{ij}$.

| Model | | $C_{11}$ | $C_{12}$ | $C_{44}$ | $S_{11}$ | $S_{12}$ | $S_{44}$ |
|---|---|---|---|---|---|---|---|
| $LaTi_2Al_{20}$ | Cal. | 141.449 | 44.034 | 66.931 | 0.0083 | –0.0020 | 0.0149 |
| $LaV_2Al_{20}$ | Cal. | 124.607 | 34.377 | 62.276 | 0.0091 | –0.0019 | 0.0161 |
| $LaCr_2Al_{20}$ | Cal. | 143.979 | 55.504 | 52.519 | 0.0088 | –0.0025 | 0.0190 |
| $LaNb_2Al_{20}$ | Cal. | 174.569 | 42.241 | 63.331 | 0.0063 | –0.0012 | 0.0158 |
| $LaTa_2Al_{20}$ | Cal. | 144.699 | 56.808 | 63.479 | 0.0089 | –0.0025 | 0.0158 |
| Al | Cal. | 112.091 | 63.424 | 32.065 | 0.0151 | –0.0055 | 0.0312 |
| Al[43] | Exp. | 124 | 61.9 | 31.6 | | | |
| Al[44] | Exp. | 109 | 64.5 | 32.4 | | | |
| Al[45] | Exp. | 108 | 62 | 28 | | | |

**Table 3.** Calculated elastic moduli (in unit GPa) $B$, $G$, $E$, $B/G$, $H_v$, and Poisson's ratio $v$.

| Model | $B$ | $G$ | $E$ | $B/G$ | $H_v$ | $v$ |
|---|---|---|---|---|---|---|
| $LaTi_2Al_{20}$ | 76.506 | 58.930 | 140.671 | 1.298 | 12.249 | 0.194 |
| $LaV_2Al_{20}$ | 64.453 | 54.732 | 127.972 | 1.178 | 12.191 | 0.169 |
| $LaCr_2Al_{20}$ | 84.996 | 49.033 | 123.375 | 1.733 | 7.747 | 0.258 |
| $LaNb_2Al_{20}$ | 86.350 | 64.450 | 154.828 | 1.339 | 12.590 | 0.201 |
| $LaTa_2Al_{20}$ | 86.105 | 54.781 | 135.588 | 1.572 | 9.359 | 0.237 |
| Al | 79.646 | 28.711 | 76.893 | 2.774 | 2.868 | 0.339 |
| Al Exp | 79.3[43] | 29.4[43] | | 2.493[45] | | 0.323[45] |

**Table 4.** Calculated bulk modulus $B_V$, $B_R$ (in unit GPa), shear modulus $G_V$, $G_R$ (in unit GPa), and elastic anisotropic factors.

| Model | $B_V$ | $B_R$ | $G_V$ | $G_R$ | $A^U$ | $A$ |
|---|---|---|---|---|---|---|
| $LaTi_2Al_{20}$ | 76.506 | 76.506 | 59.642 | 58.218 | 0.122 | 1.374 |
| $LaV_2Al_{20}$ | 64.453 | 64.453 | 55.412 | 54.052 | 0.126 | 1.380 |
| $LaCr_2Al_{20}$ | 84.996 | 84.996 | 49.206 | 48.860 | 0.035 | 1.187 |
| $LaNb_2Al_{20}$ | 86.350 | 86.350 | 64.464 | 64.435 | 0.002 | 0.957 |
| $LaTa_2Al_{20}$ | 86.105 | 86.105 | 55.665 | 53.896 | 0.164 | 1.444 |
| Al | 79.646 | 79.646 | 28.972 | 28.449 | 0.092 | 1.318 |

The ductile or brittle behavior influences the high temperature application of solid materials. The values of $B/G$ ratio and Poisson's ratio $v$ can determine the brittle and ductile behaviors of solid materials. When the values of $B/G$ and $v$ are less than 1.75 and 0.26, the solid materials possess brittle behavior. Otherwise, the solid materials possess ductile behavior. The calculated values of $B/G$ and $v$ are shown in Table 3. The values of $B/G$ and $v$ of $LaT_2Al_{20}$ intermetallics are all smaller than the critical value 1.75 and 0.26, which indicates that $LaT_2Al_{20}$ intermetallics are all brittle materials. But Al possesses the ductile behavior because of the larger $B/G$ and $v$ values (2.774 and 0.339). In the meantime, $LaV_2Al_{20}$ has the smallest $B/G$ and $v$, this indicates that it possesses the largest brittleness among these compounds. The values of elastic constants ($C_{11}$–$C_{12}$) and Young's modulus are the criterion to estimate the plasticity of solid materials. Generally speaking, if the solid materials have the smaller values of elastic constants and Young's modulus, they will possess better plasticity.[47] In order to intuitively describe the plastic behavior, the results of the $LaT_2Al_{20}$ compounds and the experimental ones for pure Al[45] are shown in Fig. 6. In Fig. 6, the pure Al has the best plasticity and $LaT_2Al_{20}$ compounds have the worse plasticity than the pure Al. In order to present the brittleness of $LaT_2Al_{20}$ compounds, figure 7 shows the renormalized hyperbolic correlation derived by $(C_{12}–C_{44})/E$ and $G/B$, including the calculated values of $LaT_2Al_{20}$ with some typical materials, Au, Pd, Al, Si, Ge, BN, diamond, and so on.[48] According to the Pugh criterion and Pettifor criterion, the $LaT_2Al_{20}$ compounds possess the brittle nature and high hardness, which is close to that of Si, Ge, and BN.

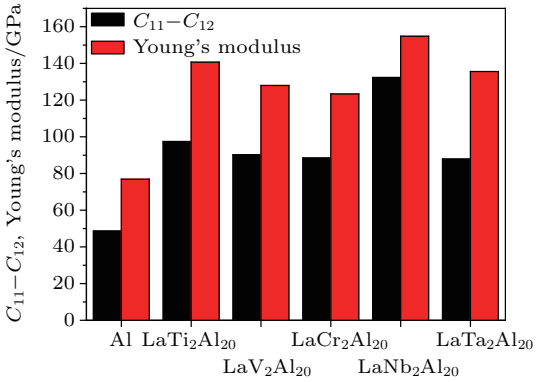



**Fig. 6.** (color online) The values of $C_{11}$–$C_{12}$ and Young's modulus for pure Al and $LaT_2Al_{20}$ intermetallics.

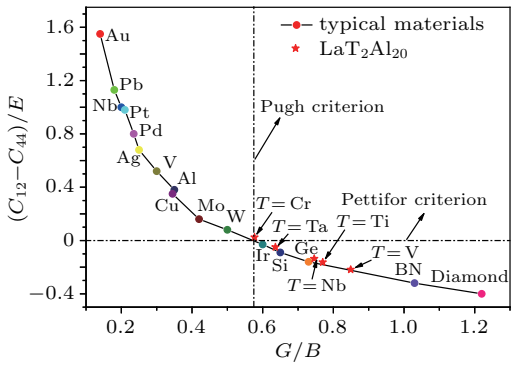



**Fig. 7.** (color online) The renormalized hyperbolic correlation derived by $(C_{12}–C_{44})/E$ and $G/B$.

### 3.3. Anisotropic properties

The anisotropic properties are closely related to the micro-cracks behavior of solid materials. The anisotropic properties were described by the universal and shear anisotropic index $A^{\mathrm{U}}$ and $A$[46]

$$A^{\mathrm{U}} = 5\frac{G_V}{G_R} + \frac{B_V}{B_R} - 6, \quad A = \frac{2C_{44}}{C_{11} - C_{12}}. \tag{5}$$

The calculated anisotropic indexes $A^{\mathrm{U}}$ and $A$ are shown in Table 4. When the anisotropic values of $A^{\mathrm{U}}$ and $A$ approach to and 1 respectively, the crystalline phases possess the isotropic properties. The anisotropic data listed in Table 4 confirm that these compounds are anisotropic. The indexes $A^{\mathrm{U}}$ and $A$ correspond to the same order: $LaTa_2Al_{20} > LaV_2Al_{20} > LaTi_2Al_{20} > Al > LaCr_2Al_{20} > LaNb_2Al_{20}$, which indicates that $LaTa_2Al_{20}$ has the largest anisotropy, but $LaNb_2Al_{20}$ possesses the smallest anisotropy. But the degree of anisotropy of $LaT_2Al_{20}$ compounds is small and $LaNb_2Al_{20}$ approaches to the isotropy.

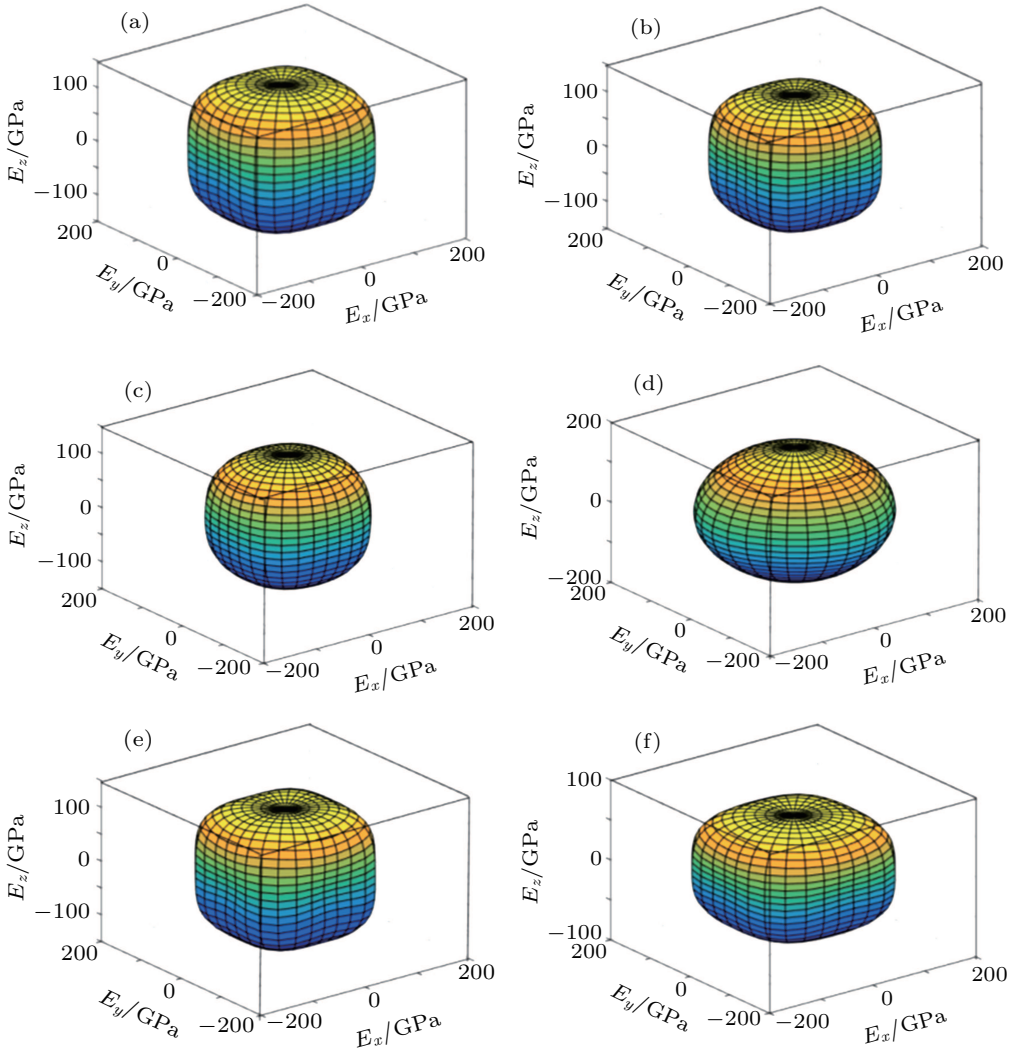



**Fig. 8.** (color online) (a)–(f) The surface contours of the Young's modulus for $LaTi_2Al_{20}$ (a), $LaV_2Al_{20}$ (b), $LaCr_2Al_{20}$ (c), $LaNb_2Al_{20}$ (d), $LaTa_2Al_{20}$ (e), and Al (f).

In order to visually describe anisotropic properties of $LaT_2Al_{20}$ intermetallics, the three-dimensional surfaces of Young's modulus $E$ was adopted to further explore the anisotropy of crystal phases. The three-dimensional (3D) figures were displayed using the following equation[46]

$$\frac{1}{E} = S_{11} - 2\left(S_{11} - S_{12} - \frac{S_{44}}{2}\right)\left(l_1^2 l_2^2 + l_2^2 l_3^2 + l_1^2 l_3^2\right). \tag{6}$$

If the 3D surfaces of Young's modulus are spherical, they will be isotropic. Otherwise, they are anisotropic. The greater the degree of deviation from the sphere is, the stronger the anisotropic properties are. The 3D figures of Young's modulus are shown in Fig. 8. According to the degree of deviation from the sphere, it can be concluded that $LaT_2Al_{20}$ intermetallics are all anisotropic. The degree of deviation from the sphere for $LaNb_2Al_{20}$ is smallest among six figures, suggesting that it is basically isotropic. On the contrary, $LaTa_2Al_{20}$ has the largest anisotropy. The figures of other compounds display the degree of deviation, but the degree of deviation is small, indicating that these intermetallics are anisotropic and

the anisotropy is small. In order to furthermore describe the anisotropic properties of the $LaT_2Al_{20}$ intermetallics, the two-dimensional figures of Young's modulus on different planes are plot in Fig. 9. If the contours of the closed curves are circles, the crystal materials possess the isotropic properties. If the contours of the closed curves deviate from circles, the crystal materials possess the elastic anisotropy. In Fig. 9, the contours of the $LaNb_2Al_{20}$ are closed to circles, but $LaTa_2Al_{20}$ and Al possess the larger degree of deviation, indicating that $LaNb_2Al_{20}$ is more closed to the elastic isotropy.

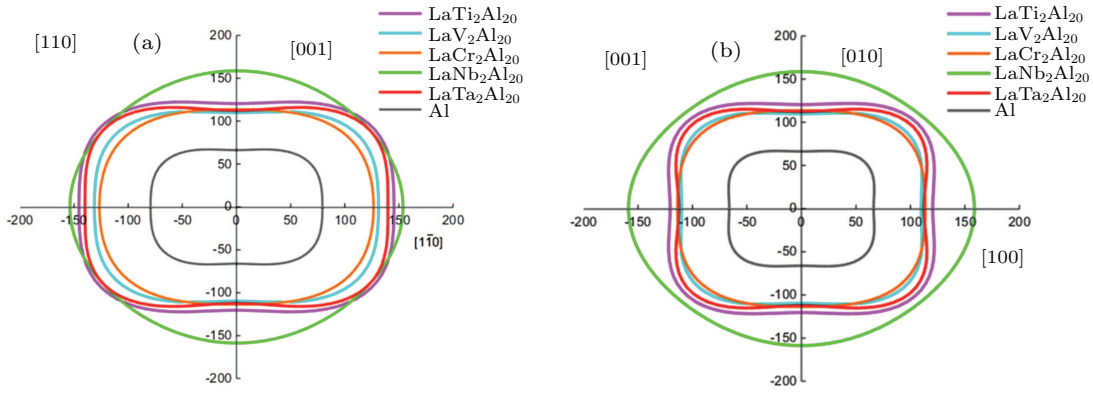



**Fig. 9.** (color online) The projections on the (001) and (110) planes of Al and $LaT_2Al_{20}$ intermetallics.

### 3.4. Electronic and magnetic properties

The total density of states (TDOS) and partial density of states (PDOS) of $LaT_2Al_{20}$ from $-12$ eV to 4 eV are shown in Fig. 10. The dash line at zero energy represents the Fermi level $E_F$ in Fig. 10. There are no energy gaps near the Fermi level $E_F$, indicating that five intermetallics exhibit metallic property. The region of energy binding states from about $-12$ eV to $-4$ eV in TDOS is determined mainly by Al 3s and 3p states. The energy binding states near the Fermi level $E_F$ are hybridized mainly by La 5d, $T$ (Ti/V/Cr) 3d, and Al 3p states. The strong hybridization creates the pseudogap near the Fermi level in TDOS for five $LaT_2Al_{20}$ intermetallics. The strong hybridization can guarantee the electronic interaction between the atoms and improve the bond strength. $LaT_2Al_{20}$ intermetallics exhibit the better elastic properties than pure Al, which is attributed to the bond strength of La–Al, La–$T$, and $T$–Al metallic bonds of $LaT_2Al_{20}$ intermetallics. Comparing the up states with the down states of TDOS in Fig. 11, we found that the spin-down and spin-up states are not symmetric for $LaCr_2Al_{20}$ intermetallics, but the spin states of other four $LaT_2Al_{20}$ ($T$ = Ti, V, Nb, and Ta) compounds are symmetric. It indicates that $LaCr_2Al_{20}$ intermetallics exhibit magnetic properties and other four $LaT_2Al_{20}$ compounds are nonmagnetic compounds. The results are consistent with the experiments ones.[17,29,31]

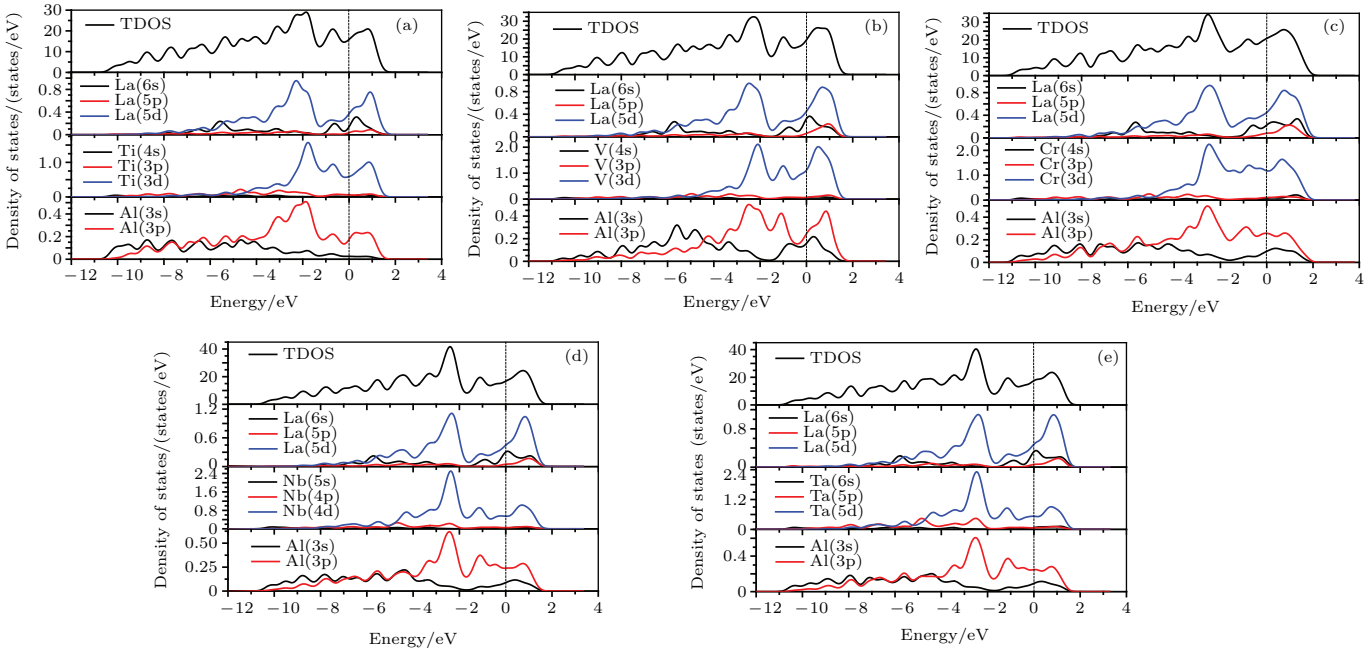



**Fig. 10.** (color online) Density of states of $LaT_2Al_{20}$ intermetallics.

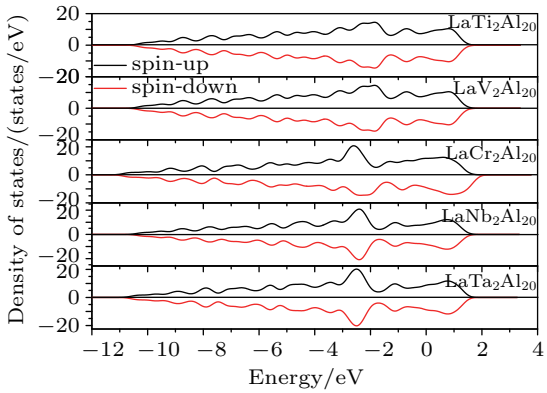



**Fig. 11.** (color online) Total density of states of spin-up and sipn-down for La$T_2$Al$_{20}$ intermetallics.

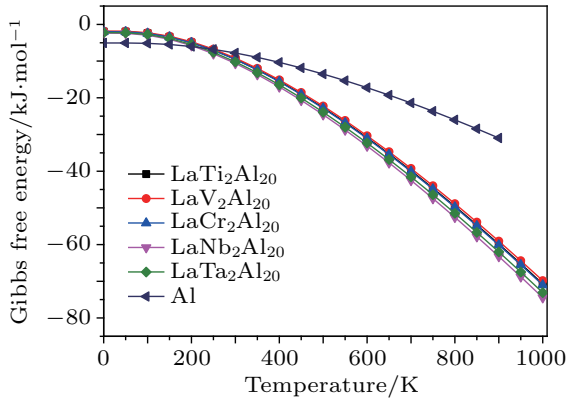



**Fig. 12.** (color online) Relationships between Gibbs free energy and temperature of pure Al and La$T_2$Al$_{20}$ intermetallics.

### 3.5. Thermodynamic properties

For cubic structural crystals, they have only one-independent lattice parameter. Thus, we performed the lattice dynamic calculations for the variable lattice parameter from 0.94$a$ to 1.06$a$ in a step of 0.01$a$ within the PHONOPY code. By using $F$ ($V$, $T$)–$V$ data, we fit them to Vinet EOS and obtained the related thermodynamic parameters. The relationships between thermodynamic quantities and temperature for pure Al and La$T_2$Al$_{20}$ intermetallics are shown in Figs. 12–15. Because the melt point temperature of Al is about 960 K, so we gave out the thermodynamic quantities between 0 K and 900 K for pure Al. Figure 12 shows the relationships between Gibbs free energy and the elevated temperature. The Gibbs free energy is negative and decreases gradually with increasing temperature, indicating that these compounds are thermodynamically stable in the whole temperature range. The smaller the Gibbs free energy is, the better the thermal stability of compound is. Five La$T_2$Al$_{20}$ intermetallics exhibit the better thermal stability than pure Al in the high temperature section. Figure 13 shows the relationships between bulk modulus and the elevated temperature. It is clear that when the temperature is less than 100 K, the bulk modulus nearly remains constant, but it drops remarkably in the high temperature section. The change of bulk modulus of La$T_2$Al$_{20}$ intermetallics is smaller than Al, indicating that the ability of creep resistance of La$T_2$Al$_{20}$ intermetallics are better than pure Al. Figure 14 shows the relationships between thermal expansion coefficients and temperature. It is noted that the expansion coefficients increase exponentially in the low temperature section and increase slowly (approaches to the linear increases) in the high temperature regime. But in the high temperature section, the values of pure Al are remarkably larger than those of five La$T_2$Al$_{20}$ compounds at a given temperature, indicating

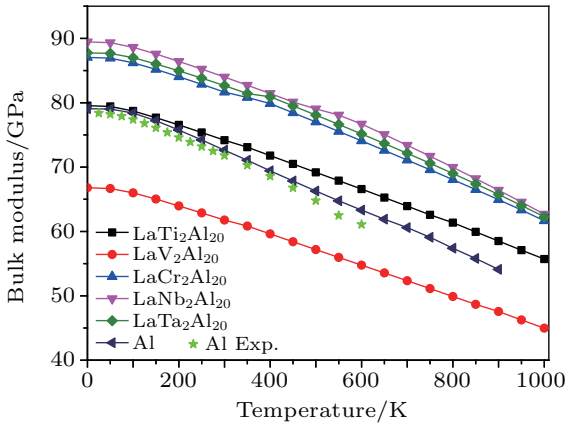



**Fig. 13.** (color online) Relationships between bulk modulus and temperature of La$T_2$Al$_{20}$ intermetallics.

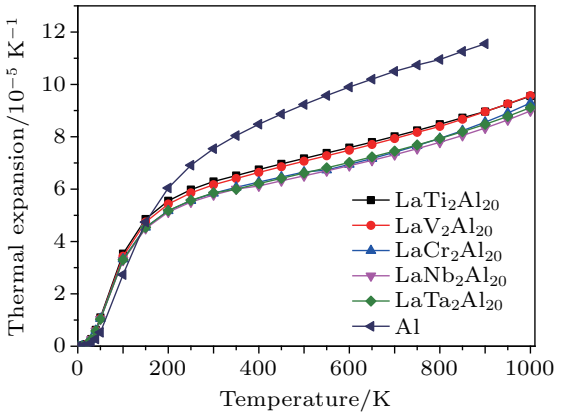



**Fig. 14.** (color online) Relationships between thermal expansion and temperature of pure Al and La$T_2$Al$_{20}$ intermetallics.

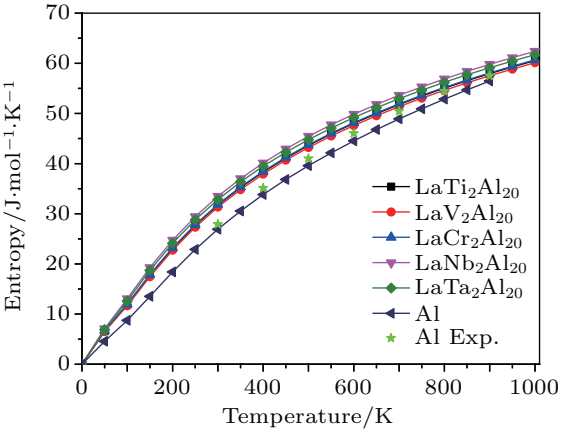



**Fig. 15.** (color online) Relationships between entropy and temperature of pure Al and La$T_2$Al$_{20}$.

that the pure Al becomes easier to expand at high temperature. Figure 15 shows the relationships between entropy and temperature. The values of entropy of pure Al and $RET_2Al_{20}$ compounds rapidly increase almost linearly with the elevated temperature. In order to prove the correctness of our calculation method, we compared the theoretical values and the experimental ones[49–51] of bulk modulus and entropy of pure Al in Figs. 13 and 15. The calculated results are very close to the experimental ones, which indicate that the calculated method and results are reliable.

## 4. Conclusions

In summary, the first-principles method is used to explore the structural stability, mechanical properties, and thermodynamic properties of pure Al and $LaT_2Al_{20}$ compounds. The calculated formation enthalpy and phonon frequencies indicate that $LaT_2Al_{20}$ intermetallics exhibit the structural stability. The elastic constants $C_{ij}$ and moduli ($B$, $G$, and $E$) indicate that $LaT_2Al_{20}$ intermetallics possess the better elastic properties than pure Al. The anisotropy in elastic constants and Young's modulus indicates that $LaT_2Al_{20}$ compounds are anisotropic. The calculated thermal quantities indicate that $LaT_2Al_{20}$ intermetallics possess the better thermal physics properties at high temperatures.

## References


[1] Schlapbach L and Züttel A 2001 *Nature* **414** 353
[2] Taend J, Orthacker A and Amenitsch H 2016 *Acta Mater.* **117** 43
[3] Yu L B, Wang J, Qu F S, Wang M and Wang W 2018 *J. Alloys Compd.* **737** 655
[4] Suwanpreecha C, Pandee P, Patakham U and Limmaneevichitr C 2018 *Mater. Sci. Eng. A* **709** 46
[5] Dorin T, Ramajayam M, Lamb J and Langanc T 2017 *Mater. Sci. Eng. A* **707** 58
[6] Tian T, Wang X F and Li W 2013 *Solid State Commun.* **156** 69
[7] Marquis E A, Seidman D N and Dun, D C 2002 *Acta Mater.* **50** 4021
[8] Iwamura S and Miura Y 2004 *Acta Mater.* **52** 591
[9] Mikhaylovskay A V, Mochugovskiy A G, Levchenko V S and Mufalo W 2018 *Mater. Charact.* **139** 30
[10] Chen Z, Zhang P, Chen D, Wu Y and Wang M 2015 *J. Appl. Phys.* **117** 085904
[11] Clouet E, Barbu A, La L and Martin G 2005 *Acta Mater.* **53** 2313
[12] Vo N Q, Dun, D C and Seidman D N 2014 *Acta Mater.* **63** 73
[13] Spierings A B and Dawson K 2017 *Mater. Design* **115** 52
[14] Lin J D, Okle P and Dun D C 2017 *Mater. Sci. Eng. A* **680** 64
[15] Wen S P, Wang W and Zhao W H 2016 *J. Alloys Compd.* **687** 143
[16] Halevy I, Sterer E, Aizenshtein M, Kimmel G, Regev D and Yahel E 2001 *J. Alloys Compd.* **319** 19
[17] Yamada A, Higashinaka R, Matsuda T D and Aoki Y 2018 *J. Phys. Soc. Jpn.* **87** 033707
[18] Bram A I, Venkert A and Meshi L 2015 *J. Alloys Compd.* **641** 1
[19] Wakiya K, Onimaru T and Matsumoto K T 2017 *J. Phys. Soc. Jpn.* **86** 3
[20] Winiarski M J, Griveau J C, Colineau E and Wochowski K 2017 *J. Alloys Compd.* **696** 1113
[21] Liu P C, Xian Y J, Wang X, Zhang Y T and Zhang P C 2017 *J. Nucl. Mater.* **493** 147
[22] Winiarski M J and Klimczuk T 2017 *J. Solid State Chem.* **245** 10
[23] Moussa C, Berche A, Pasturel M, Barbosa J, Stepnik B, Dubois and Tougait O 2017 *J. Alloys Compd.* **691** 893
[24] Winiarski M J and Klimczuk T 2017 *Intermetallics* **85** 103
[25] Winiarski M J, Wiendlocha B, Sternik M, Winiewski P, O'Brien J R, Kaczorowski D and Klimczuk T 2016 *Phys. Rev. B* **93** 134507
[26] Sakai A and Nakatsuji S 2011 *Phys. Rev. B* **84** 201106
[27] Swatek P and Kaczorowski D 2016 *J. Magn. Magn. Mater.* **416** 348
[28] Tsujimoto M, Matsumoto Y, Tomita T, Sakai A and Nakatsuji S 2014 *Phys. Rev. Lett.* **113** 267001
[29] Kumar K R, Nair H S, Christian R, Thamizhavel A and Strydom A M 2016 *J. Phys.: Condens. Matter* **28** 436002
[30] Verbovytsky Y, Latka K and Tomala K 2007 *J. Alloys Compd.* **442** 334
[31] Kangas M J, Schmitt D C, Sakai A, Nakatsuji S and Chan J Y 2012 *J. Solid State Chem.* **196** 274
[32] Thiede V M T, Jeitschko W, Niemann S and Ebel T 1998 *J. Alloys Compd.* **267** 23
[33] Kresse G and Joubert D 1999 *Phys. Rev. B* **59** 1758
[34] Togo A and Tanaka I 2015 *Scr. Mater.* **108** 1
[35] Shang S, Wang Y and Liu Z K 2007 *Appl. Phys. Lett.* **90** 101909
[36] Pan Y and Guan W M 2018 *Ceram. Int.* **44** 9893
[37] Pan Y, Guan W M and Li Y Q 2018 *Phys. Chem. Chem. Phys.* **20** 15863
[38] Song Y, Zuo X and Yue Y L 2018 *Chin. Phys. B* **27** 037102
[39] Li Y, Dai X F, Liu G D, Wei Z Y, Liu E K, Han X L, Du Z W, Xi X K, Wang W H and Wu G H 2018 *Chin. Phys. B* **27** 026101
[40] Liu D R, Han D, Huang M L, Zhang X, Zhang T, Dai C M and Chen S Y 2018 *Chin. Phys. B* **27** 018806
[41] He W Q, Huang H B, Liu Z H and Ma X Q 2018 *Chin. Phys. B* **27** 016201
[42] Stedman R and Nilson G 1966 *Phys. Rev.* **145** 492
[43] Li Z and Tse J S 2000 *Phys. Rev. B* **61** 14531
[44] Mao Z, Chen W, Seidman D N and Wolverton C 2011 *Acta Mater.* **59** 3012
[45] Grimvall G 1999 *Thermo Physical Properties of Materials* (Amsterdam: North Holland) p. 256
[46] Chen S, Sun Y, Duan Y H, Huang B and Peng M J 2015 *J. Alloys Compd.* **630** 202
[47] Hu W C, Liu Y, Li D J, Zeng X Q and Xu C S 2013 *Physica B* **427** 85
[48] Niu H Y, Chen X Q, Liu P T, Xing W W, Cheng X Y and Li D Z 2012 *Sci. Rep.* **2** 718
[49] Vinet P, Rose J, Ferrante J and Smith J 1989 *J. Phys.: Condens. Matter* **1** 1941
[50] Wallace D C 1972 *Thermodynamics of Crystals* (New York: Dover) p. 241
[51] Barin I 1995 *Thermochemical Data of Pure Substance* (Beijing: Science Press) p. 528